HHS Public Access

Author manuscript

Dev Biol. Author manuscript; available in PMC 2021 April 15.

Published in final edited form as:

Dev Biol. 2020 April 15; 460(2): 187–199. doi:10.1016/j.ydbio.2019.12.014.

Loss of ciliary transition zone protein TMEM107 leads to heterotaxy in mice

Natalia A. Shylo[*,1], **Elli Emmanouil**, **Dylan Ramrattan**, **Scott D. Weatherbee**

Yale University, Genetics Department, 333 Cedar Street, New Haven, CT, 06510, USA

Abstract

Cilia in most vertebrate left-right organizers are involved in the original break in left-right (L-R) symmetry, however, less is known about their roles in subsequent steps of the cascade – relaying the signaling and maintaining the established asymmetry. Here we describe the L-R patterning cascades in two mutants of a ciliary transition zone protein TMEM107, revealing that near-complete loss of cilia in *Tmm107*^{nul1} leads to left pulmonary isomerism due to the failure of the midline barrier. Contrary, partially retained cilia in the node and the midline of a hypomorphic *Tmem107*^{schlei} mutant appear sufficient for the formation of the midline barrier and establishment and maintenance of the L-R asymmetry. Despite misregulation of *Shh* signaling in both mutants, the presence of normal *Lefty1* expression and midline barrier formation in *Tmem107*^{schlei} mutants, suggests a requirement for cilia, but not necessarily *Shh* signaling for *Lefty1* expression and midline barrier formation.

Keywords

Left-right asymmetry; TMEM107; Cilia; Midline barrier; Shh

1. Introduction

Heterotaxy, an abnormal, often randomized, formation and arrangement of internal organs along the left-right (L-R) axis, typically involves severe cardiac abnormalities, associated with a high mortality rate (Kim, 2011; Lin et al., 2014). Mouse models have been essential to discern the function of genes mutated in patients and identify new heterotaxy loci (Li et al., 2015; Norris and Grimes, 2012). Among known heterotaxy-associated genes many are involved in cilia formation and function (Li et al., 2015; Pennekamp et al., 2015). Motile cilia in the left-right organizer (node in mouse, gastrocoel roof plate in frog, Kupffer's vesicle in zebrafish) create a leftward flow of extraembryonic fluid that breaks bilateral L-R symmetry. Mutations in ciliary dyneins that lead to paralyzed cilia, as in *Dnah11*^{iv} mutant mice, or as seen in patients with primary ciliary dyskinesia, result in randomized L-R

[*]Corresponding author. 1000 E 50th Street, Kansas City, MO, 64110, USA. NShyloHyson@stowers.org (N.A. Shylo).
[1]Stowers Institute for Medical Research, 1000 E 50th Street, Kansas City, MO 64110.

Declaration of competing interest

The authors declare no competing or financial interests.

Appendix A. Supplementary data

Supplementary data to this article can be found online at https://doi.org/10.1016/j.ydbio.2019.12.014.

patterning, including left and right isomerism – left or right bilaterally symmetric organs, respectively (Dougherty et al., 2016; Layton, 1976; Piedra et al., 1998; Seo et al., 1992; Suppet al., 1997). Sensation of flow by cilia on the crown cells of the node is necessary for degradation of *Dand5* mRNA in the crown cells at the left of the node, which relieves DAND5 inhibition of *Nodal* expression in these cells and ultimately leads to the induction of the left-side determinant *Nodal* in the left lateral plate mesoderm (LPM) (Marques et al., 2004; Yoshiba et al., 2012). Mice harboring mutations in the ciliary-localized putative calcium channel Polycystin2 (PC2, encoded by *Pkd2*) fail to induce *Nodal* in the left LPM due to their inability to sense flow (Yoshiba et al., 2012), and thus develop two right sides (Pennekamp et al., 2002).

Mounting evidence suggests that cilia have roles in L-R patterning beyond inducing and sensing the flow at the node. For example, loss of genes critical for ciliary assembly, like *Kif3a, Ift172, Ift88* and *Ift38*, results in bilateral expression of leftness markers in the LPM, while current models would instead predict right isomerism due to a failure to generate and sense the flow, and induce the Nodal cascade (Botilde et al., 2013; Grimes et al., 2016; Huangfu et al., 2003; Murcia et al., 2000; Takeda et al., 1999). Furthermore, loss of cilia is epistatic to the loss of *Pkd2*, as evidenced by left isomerism in $Kif3a^{null}; Pkd2^{null}$ embryos (Grimes et al., 2016), indicating a role for cilia downstream of flow sensation by PC2.

The ciliary transition zone (TZ) is a region at the base of the cilium, responsible for the mediation of ciliary protein composition. Defects in TZ components result in abnormal ciliary protein localization, and typically, an overall reduced number of cilia (Garcia-Gonzalo et al., 2011; Shylo et al., 2016). Disruptions of L-R patterning have been observed in mice harboring mutations in TZ protein-encoding genes, including *Rpgrip1L* (Vierkotten et al., 2007), *Tctn1, Tctn2* and *Tmem67* (Garcia--Gonzalo et al., 2011), *Mks1* (Weatherbee et al., 2009) as well as *B9d1* (Dowdle et al., 2011). However, none of these reports offer a thorough examination of the molecular basis for the L-R phenotypes occurring in these transition zone protein mutants.

Previously described $Tmem107^{schlei}$ mouse mutants, and human patients with mutations in *TMEM107*, which encodes a TZ protein, display fewer and abnormally shaped cilia, but no L-R patterning defects have been reported (Christopher et al., 2012; Lambacher et al., 2016; Shaheen et al., 2015; Shylo et al., 2016; Weatherbee et al., 2009). In this study we report that $Tmem107^{tm1Lex}$ mice that completely lack the *Tmem107* gene product (hereafter referred to as $Tmem107^{null}$) (Tang et al., 2010), have bilateral *Nodal* expression in the LPM, which underlies left pulmonary isomerism, a molecular phenotype that largely resembles mutants with a global loss of cilia. We took advantage of the $Tmem107^{schlei}$ and $Tmem107^{null}$ mutants and their differences in L-R patterning phenotype to examine additional roles for cilia in establishing the L-R axis. We show that although both $Tmem107^{null}$ and $Tmem107^{schlei}$ mutants lack cilia in the endoderm at e8.0, presence of a robust population of cilia in the nodes and midlines of $Tmem107^{schlei}$ animals is sufficient for normal establishment of the Nodal cascade. These results expand our understanding of limited observations in several other TZ mutants that develop left pulmonary isomerism and/or bilateral expression of markers in the LPM (Abdelhamed et al., 2015; Garcia-Gonzalo et al.,

2011; Vierkotten et al., 2007), but also advance our knowledge toward deeper understanding of cilia roles in L-R patterning through establishment of the midline barrier.

2. Results

2.1. Tmem107^{null} mutants display multiple left-right defects

Tmem107 encodes a ciliary transition zone protein, required for the formation of a functional transition zone in primary cilia (Lambacher et al., 2016; Shylo et al., 2016). Given the ubiquitous nature of primary cilia, we were surprised to see an enrichment of *Tmem107* mRNA in the embryonic node at E7.5–8.5, compared to all other embryonic tissues (Fig. 1 A, B and Fig. S1), suggesting a possible role for TMEM107 in the node at this early stage. This expression pattern also appeared at odds with the lack of L-R abnormalities in a previously described ENU-induced *Tmem107*^{schlei} mouse mutant (Christopher et al., 2012). However, close examination of the Tmem107^{null} mutant (Tang et al., 2010), revealed multiple heterotaxy characteristics, including randomized heart looping and stomach positioning, as well as left isomerism of the lungs (Fig. 1 C–L and Table S3). These data indicate that TMEM107 is critical for establishing the L-R axis and that *Tmem107*^{schlei} is a hypomorphic allele. To determine the extent to which TMEM107 regulates L-R patterning we further examined the heterotaxy phenotype in *Tmem107*^{null} mutants.

The position of the heart apex was used to determine directionality of heart looping and reveal its randomization. About a quarter of *Tmem107*^{null} mutants (n = 6/26) showed clear, abnormal right-side looping of the heart, with another quarter exhibiting ambiguous looping, without clear apex positioning towards left or right (n = 6/26) (Fig. 1 C–F, red arrows in D–F). Stomach positioning appeared to be independent of heart directionality and showed perfect randomization in *Tmem107*^{null} embryos compared to the normal left-sidedness (Fig. 1 C, Table S3). We also examined the developing lungs, which, in control mice, form one lobe on the left side, and four lobes on the right side (Fig. 1 C, G, J). The lungs in *Tmm107*^{null} embryos were bilaterally single-lobed (Fig. 1 C, H, I, K, L). Careful examination of E13.5 lungs revealed that both single lobes had equivalent numbers of branching points, consistent with normal branching pattern for the left lobe at that stage (Metzger et al., 2008) (Fig. 1 C, G–I). This could potentially result from a developmental delay in the lung lobation of the right lung. However, at later stages, we observed that *Tmem107*^{null} lungs maintain single lobes on each side, in addition to becoming severely hypoplastic, (Fig. 1 C, J–L). Overall, we conclude that *Tmem107*^{null} embryos develop left pulmonary isomerism (Fig. 1 C, G–L).

2.2. L-R perinodal signaling is disrupted in Tmem107^{null} mutants

Left-right patterning of the organs begins at the node, and the earliest marker of the L-R symmetry break is degradation of *Dand5* mRNA on the left side of the node in response to cilia-generated flow (Inacio et al., 2013; Kawasumi et al., 2011; Marques et al., 2004; Nakamura et al., 2012; Schweickert et al., 2010; Shinohara et al., 2012). Left-side *Dand5* degradation is apparent by 2–3 somites stage in controls and becomes more pronounced at the 4–5 somites stage (Fig. 2 A, B, E). In contrast, *Dand5* expression in *Tmem107*^{null} embryos is bilateral and equal at the 2–3 somites stage, and either maintains equal bilateral

expression, or becomes degraded in a random fashion by 4–5 somites stage (Fig. 2 C, D, F). Normally, left-sided *Dand5* degradation alleviates its inhibition of *Nodal*, and leads to subsequent *Nodal* upregulation on the left side of the node (Fig. 2 G, H, K). We expected that the equal bilateral *Dand5* expression would lead to bilateral down-regulation of *Nodal* (Marques et al., 2004), but we observed randomized *Nodal* expression levels around *Tmem107*^{null} nodes (Fig. 2I–L). These results suggest a disconnect between the expression of *Dand5* and *Nodal* in the nodes of *Tmem107*^{null} embryos, but appear to be in line with some other similar reports in the literature (Ishimura et al., 2008; Marques et al., 2004; Norris et al., 2002).

2.3. Nodes of Tmem107^{null} embryos have cilia with motile identity

Dand5 degradation is dependent on the ability to sense nodal flow (Nakamura et al., 2012; Schweickert et al., 2010), so the lack of early left-sided *Dand5* degradation points to abnormal motile cilia in the pit of the node or flow sensing cilia surrounding the node. We used ARL13B as a marker of cilia, and discovered that the nodes of E8.0 (2–5 somites) *Tmem107*^{null} embryos were the only region where we detected ARL13B + cilia, as compared to extensive ARL13B + cilia throughout control embryos (Fig. 3 A–F – high magnification of representative nodes (4 somites), S2 A–D, G–J – low magnification). However, *Tmem107*^{null} mutant nodes had significantly ($p < 0.0001$) fewer cilia (mean = 75), as compared to controls (mean = 226) (Fig. 3 I), which is consistent with overall cilia number reductions reported in *Tmem107*^{schlei} mouse mutants, and in human patients with mutations in *TMEM107*. (Christopher et al., 2012; Lambacher et al., 2016; Shaheen et al., 2013; Shylo et al., 2016). We also discovered that cilia in the nodes of *Tmem107*^{null} mutants were significantly shorter than in control nodes (null mean = 1.811 μm, control mean = 2.568 μm, $p < 0.0001$) (Fig. 3 J). This result presents a deviation from previously published observations of longer primary cilia in cell cultures, derived from patients with mutations in *Tmem107* (Lambacher et al., 2016; Shaheen et al., 2013; Shylo et al., 2016).

The loss of ARL13B + cilia in the endoderm, surrounding the node (Fig. 3 A, B, S2 A–D, G–J) stands in contract with the specific enrichment of *Tmem1*07 mRNA in the node. These data indicate that TMEM107 is required throughout the embryo and, in addition to its specific enrichment at the node (Fig. 1 A, B, S1); *Tmem107* must be expressed in other tissues, but below the detection levels of *in situ* hybridization.

To test whether *Tmem107*^{null} mutants lack cilia with motile identity specifically, we introgressed a transgenic reporter for an axonemal dynein required for ciliary motility, *Dnah11*, fused to *GFP* (*Dnah11-GFP*) (McGrath et al., 2003). All cilia in the pit of control nodes are DNAH11-GFP + (Fig. 3 K, M, O). We found that most cilia in the pit of *Tmem107*^{null} nodes are also DNAH11- GFP + (Fig. 3 L, N, P) indicating that cilia with motile identity are specified in the absence of TMEM107 function. These results show that there is a capacity to make motile cilia. However, these cilia are shorter than normal (Fig. 3 J), and shorter motile cilia in the zebrafish Kupffer's vesicle have been linked to reduced ciliary velocity, slower flow, and L-R patterning defects, a likely scenario in *Tmem107*^{null} nodes (Lopes et al., 2010).

The positioning of motile cilia in the node can also affect the efficiency of flow, and the resultant break in L-R symmetry. Planar cell polarity pathway (PCP) drives the positioning of the cilium to the posterior end of the cells in the node by late headfold stage (Hashimoto et al., 2010), which tilts them, and ultimately creates leftward-directed flow (Nonaka et al., 2005). Disrupted ciliary positioning in the nodal cells leads to randomization of L-R situs (Mahaffey et al., 2013; May-Simera et al., 2010; Song et al., 2010). We evaluated the positioning of cilia in *Tmem107*^{null} nodal pit cells along the anterior-posterior axes, and found that they are, indeed, located posterior to the center of the cell, similar to control (Fig. S2 N). Therefore, it seems that TMEM107 is not involved in PCP, and does not regulate ciliary positioning in the cell.

2.4. Nodes of Tmem107^{null} embryos retain cilia with sensory identity

To examine whether the *Tmem107*^{null} nodes have sensory cilia, we next examined the localization of PC2, which is enriched in crown cells surrounding the node and is required for flow sensing (Yoshiba etal., 2012)We observed many PC2 + cilia in *Tmem107*^{null} crown cells, suggesting that ciliated cells with flow-sensing identity are preserved in the mutants (Fig. 3 G, H – high magnification, S2E, F, K, L – low magnification of representative nodes). The absolute numbers of PC2 + cilia in *Tmem107*^{null} nodes was lower than in control nodes (null mean = 66.4 cilia vs control mean = 136.5 cilia, $p \leq 0.0125$), however, proportionately to the overall numbers of cilia counted, roughly 60% of control cilia were both Arl13b + and PC2+, compared to 80% of *Tmem107*^{nul} cilia. Thus, nodes of *Tmem107*^{null} embryos maintain both cilia with motile and sensory identities, albeit at significantly decreased numbers and with altered morphology.

We were interested to test whether the remaining PC2+ cilia in *Tmem107*^{null} embryos are functional. In a genetic epistasis experiment, we analyzed the patterning and the numbers of lobes in the lungs of animals with a loss of *Tmem107* and *Pkd2* as a readout of the downstream L-R signaling that occurs in these animals. The four classes of phenotypes we observed were (1) normal (Fig. 3 Q), (2) left isomerism (Fig. 3 R), (3) right isomerism (Fig. 3 S), and (4) ambiguous (Fig. 3 T). Lungs deemed ambiguous included a range of phenotypes, most having some partial lobation on both sides, without being a clear right or left isomerism.

Pkd2^{null} mutant animals are typically reported to display right pulmonary isomerism due to their inability to sense nodal flow and relay that information to the LPM, thus failing to express *Nodal* and its downstream targets in the LPM (Grimes et al., 2016; Pennekamp et al., 2002). In our crosses, we used *Pkd2*^{tm2Som} mice, herein referred to as *Pkd2*^{null} (Wu et al., 1998). Most *Tmem107* ^{wt}; *Pkd2*^{null} animals analyzed displayed right isomerism, consistent with other observations in the literature (Fig. 3 U, Table S4). However, a small subset of animals had more ambiguous lungs. Furthermore, a loss of a single copy of *Tmem107* appeared to exacerbate this phenotype. Most *Tmem107*^{het}; *Pkd2*^{null} animals had ambiguous lungs, and some even presented with left isomerism (Fig. 3 U, Table S4). These data were more consistent with randomized and bilateral *Pitx2* observed in *Pkd2*^{tm1Dwo} mutants, also presumed to be null (Pennekamp et al., 2002; Yoshiba et al., 2012). Overall, these observations point to susceptibility of the right isomerism phenotype in *Pkd2*^{null}

animals to background differences and modifier genes, a phenomenon previously reported in the human population (Harris and Rossetti, 2010). Most importantly, these early observations suggested a genetic interaction between *Tmem107* and *Pkd2*. We further found that *Tmem107*^{null}; *Pkd2*^{null} animals have left isomerism, most similar to *Tmem107*^{null}; *Pkd2*^{wt} animals (Fig 1 C, G–L, Fig. 3 U, Table S4).

These observations rise some key points. First, this phenotype is reminiscent of the bilateral *Pitx2* phenotype, previously observed in *Kif3a*^{null}; *Pkd2*^{null} mutant that lacks cilia (Grimes et al., 2016), suggesting that *Tmem107*^{null} mutant largely behaves as a loss of cilia mutant. Lungs cannot be evaluated in *Kif3a*^{null}; *Pkd2*^{null} mutant animals due to their early lethality. Secondly, our original question of whether the remaining PC2+ cilia in *Tmem107*^{null} embryos are functional remains unanswered due to the epistatic relationship between *Tmem107* and *Pkd2*. Together, our data suggest that TMEM107 has significant roles in L-R patterning downstream of the flow sensing event.

It is probable that short motile cilia in *Tmem107*^{null} nodes generate only weak leftward flow, and may even have randomized flow. However, the roles for TMEM107 downstream of ciliary involvement at the node override any potential phenotype that arises at the node. Given these observations, the remainder of these studies focus on the roles of cilia and *Tmem107* in the late stages of establishing and maintaining L-R asymmetry.

2.5. Nodal and Pitx2 are expressed bilaterally in the lateral plate mesoderm of Tmem107^{null} embryos

Asymmetric *Nodal* at the node is thought to signal to the lateral plate mesoderm (LPM) and autoactivate robust *Nodal* expression specifically in the left LPM (Fig. 4. A, C), (Kawasumi et al., 2011; Yamamoto et al., 2003). *Nodal* expression in the left LPM is transient, starting around the 2–3 somites stage, and becomes extinguished a few hours later (6–7 somites stage). To test if there were defects in the transmission of the NODAL signal from the node to the LPM, we examined *Nodal* LPM expression between 0–5 somites (Fig. 4 A–C). Consistent with the lung phenotype, the vast majority of *Tmem107*^{null} embryos displayed bilateral *Nodal* transcripts in the LPM (Fig. 4 B, C) by 4–5 somites stage. Interestingly, a closer inspection of *Tmem107*^{null} embryos with bilateral nodal expression revealed that 7 of 8 embryos showed unequal expression between the two sides, with 6 having higher expression on the left side, and lower on the right (Fig. 4 B, C). These data and our observations of randomized *Nodal* at the node (Fig. 2 G–L) are consistent with previous reports of dissociation between *Nodal* expression at the node and its expression in the LPM in other mutants, although the mechanism by which this occurs is unclear (Ishimura et al., 2008; Marques et al., 2004; Norris et al., 2002).

In the left LPM, NODAL signaling induces the expression of *Pitx2*, a transcription factor, whose left-side expression persists in various LPM-derived tissues, long after *Nodal* expression is lost (Fig. 4 D–F) (Lin et al., 1999; Meno et al., 1998; Ryan et al., 1998; Yoshioka et al., 1998). We observed bilateral expression of *Pitx2* in the LPM of *Tmem107*^{null} embryos, indicating that once left-side identity is established in the LPM by NODAL, it is transduced accordingly (Fig. 4 E, F). Together, the *Nodal* and *Pitx2* expression

patterns are consistent with the left pulmonary isomerism that we observe in older *Tmem107*^{null} embryos (Fig. 1 G–L).

2.6. Tmem107^{null} embryos have a defective barrier and disrupted SHH signaling in the midline

Consistently bilateral *Nodal* and *Pitx2* expression in the LPM of *Tmem107*^{null} embryos led us to examine additional factors that regulate L-R identity. The midline barrier model postulates that *Lefty1*, a TGFβ family member expressed in the left prospective floorplate (Meno et al., 1997), is required to inhibit the passage of NODAL to the right side of the embryo, preventing NODAL from autoactivating its expression in the right LPM (Meno et al., 1998; Yamamoto et al., 2003). Thus, bilateral *Nodal* expression in the LPM is a frequent indicator of the failure of the midline barrier. Additionally, broader *Nodal* expression in the left LPM than in the right may suggest that the signal from the node is originally propagated correctly, with the induction of Nodal in the left LPM, but due to the lack of the midline barrier, NODAL is able to auto activate in the right LPM as well (Nakamura et al., 2012).

In contrast to control embryos, none of the *Tmem107*^{null} mutants expressed *Lefty1* in the midline (Fig. 5 B, C, arrowheads). The absence of *Lefty1* expression, in conjunction with bilateral, frequently asymmetric (L > R) (Fig. 4 A–C), *Nodal* expression in the LPM indicates the loss of a functional midline barrier. As *Lefty1* expression has been shown to be dependent on SHH signaling (Tsiairis and McMahon, 2009; Tsukui et al., 1999), we examined SHH signaling in the midline of *Tmem107*^{null} embryos.

Hedgehog signaling is tightly linked to cilia in vertebrates, and our previous studies showed reduced SHH signaling in the neural tubes of *Tmem107*^{schlei} mutants (Christopher et al., 2012). At E8.0, *Shh* is expressed in the node and the notochordal plate (Fig. S3 A–D) (Echelard et al., 1993; Zhang et al., 2001). and SHH signaling is necessary to specify the floor plate and establish the midline (Chiang et al., 1996). We did not observe any difference in midline *Shh* expression *Tmem107*^{null} embryos (Fig. 5 D–F, Fig. S3 A, B). Both notochord and prospective floor plate are marked by robust *Shh* signal (Fig. S3 A, B). We then decided to look downstream of the ligand at the expression of two direct targets of SHH signaling, *FoxA2* (Fig. 5 G–I) and *Ptch1* (Fig. S4 A–C), which are both enriched in control midlines. Despite the normal expression of *Shh*, the midline enrichment of both *FoxA2* and *Ptch1* was reduced in all *Tmem107*^{null} embryos examined (Fig. 5 H, I, Fig. S4 B, C, arrowheads). The effect was more dramatic for *FoxA2* reduction, but was consistently observed for both probes. These results are consistent with the requirement for TMEM107 for the transduction of the midline SHH signal, and to establish *Lefty1* expression and midline barrier function.

2.7. Analysis of hypomorphic Tmem107^{schlei} embryos with normal L-R patterning reveals SHH-independent expression of Lefty 1

We previously reported that the hypomorphic *Tmem107*^{schlei} mutants did not show any disruptions in L-R asymmetry, but displayed abnormal SHH signaling in limbs and neural tubes (Christopher et al., 2012). Consistent with this, the most downstream marker of left-side patterning, *Pitx2*, is restricted to the left LPM of *Tmem107*^{schlei} mutants, similar to control embryos (Fig. 6 A–C, J, K). *Shh* was also expressed normally in the node and

midline region of all *Tmem107*^{schlei} embryos examined, including both the notochord and the prospective floor plate (Fig. 6 D–F, S3 C, D). In contrast, *FoxA2* was lost from *Tmem107*^{schlei} mutant midlines, similar to *Tmem107*^{null} embryos, and consistent with abnormal SHH signaling observed in other *Tmem107*^{schlei} tissues (Fig. 6 G–I) (Christopher et al., 2012). Notably, we detected consistent *Lefty1* expression in the midline region of *Tmem107*^{schlei} embryos (Fig. 6 J–L). These data indicate that the mutant TMEM107 protein produced by the *Tmem107*^{schlei} hypomorphic allele is sufficient for the expression of *Lefty1*, but not *FoxA2*, and is capable of establishing a midline barrier and preserving L-R identity. More specifically, they point to potential differences in SHH sensitivity between *FoxA2* and *Lefty1*.

2.8. Presence of midline cilia correlates with a functional midline barrier

TMEM107 is required for normal cilia number and ciliary protein localization (Christopher et al., 2012; Cui et al., 2011; Lambacher et al., 2016; Shaheen et al., 2013; Shylo et al., 2016; Weatherbee et al., 2009). The abnormal midline gene expression patterns in *Tmem107*^{null} mutant suggest TMEM107 may be required for cilia formation or function in the midline. Prior studies by scanning electron microscopy (SEM) and our analysis via immunofluorescence show normal cilia numbers and length in the nodes of *Tmem107*^{schlei} embryos (Fig. S5 and (Christopher et al., 2012)). However, *Tmem107* mutant midlines have not been analyzed at E8.0 for the presence of cilia.

Examination of the ARL13B cilia marker in *Tmem107*^{null} embryos revealed very few midline cilia (Fig. 7 B, B′, E, E′) compared to controls (Fig. 7 A, A′, D, D′), consistent with the low numbers of cilia in the *Tmem107*^{null} nodes, and the reports that node cells migrate into the midline and contribute to the notochordal plate (Brennan et al., 2002; Lee and Anderson, 2008; Sulik et al., 1994). Although we observed very few cilia in the nodes of *Tmem107*^{null} embryos (Fig. 3 I), their almost complete absence in the midline was surprising. Unlike *Tmem107*^{null} mutants, *Tmem107*^{schlei} embryos appear to have a normal numbers of cilia in their nodes (Fig. S5 H and (Christopher et al., 2012)) and the midlines of these animals contain high numbers of ciliated cells (Fig. 7 C, C′, F, F'). Notably, cilia are still absent from the definitive endoderm in *Tmem107*^{schlei} embryos (Fig. 7 C), suggesting a differential requirement for TMEM107 function in primary cilia of distinct embryonic tissues, and that despite the enrichment for *Tmem107* transcript at the node, the definitive endoderm is more sensitive to the *Tmem107*^{schlei} mutation. Together our findings suggest that loss of midline cilia may drive left isomerism through the loss of midline barrier function in *Tmem107*^{null}.

3. Discussion

3.1. Transition zone protein TMEM107 exhibits functional specificity in different cilia types

The transition zone is a structurally complex and protein-rich domain of the cilium, and has been the focus of significant investigation in the ciliary field (Garcia-Gonzalo and Reiter, 2017; Lambacher et al., 2016; Szymanska and Johnson, 2012; Yang et al., 2015). Since cilia are ubiquitous organelles, and a transition zone is a mandatory structural component of any

cilium, it would be expected for associated ciliary proteins to be expressed ubiquitously. As such, TMEM107 is expressed in all tissues examined (Christopher et al., 2012; Tang et al., 2010). Thus, it came as a surprise to see a strong *Tmem107* enrichment in the nodes of developing embryos. At later stages, *Tmem107* also shows strong enrichment in other tissues, including the choroid plexus, as well as olfactory and respiratory epithelia (Diez-Roux et al., 2011). All these tissues have motile cilia, suggesting a specific role for TMEM107, associated with ciliary motility.

Despite *Tmem107* enrichment in the node, motile cilia appear to be more tolerant of mutations in *Tmem107*. *Tmem107*^{schlei} nodes and midlines have high numbers of cilia and no L-R patterning defects (Fig. 7 G). *Tmem107*^{null} mutants have a nearly complete loss of cilia, but do retain some in the node (Fig. 7 G). In contrast, primary cilia are more susceptible to disruptions in *Tmem107*, and are lost in both *Tmm107*^{null} and *Tmm107*^{schlei} embryos (Fig. 7 G). Overall, it has now been shown that TMEM107 is important for ciliary formation both in humans (Lambacher et al., 2016; Shaheen et al., 2015; Shylo et al., 2016) and mice (Christopher et al., 2012). Longer primary cilia have been reported in cultures of primary human fibroblasts, derived from patients with mutations in *TMEM107* (Lambacher et al., 2016; Shaheen et al., 2015; Shylo et al., 2016). However, the remaining cilia in *Tmem107*^{null} nodes, positive for motility markers, are significantly shorter than in control embryos. Thus, it appears that TMEM107 is important for ciliary formation both in motile and primary cilia, likely through its requirement for ciliary length regulation.

3.2. Loss of Tmem107 results in disruption in early L-R patterning events at the node

The shorter cilia in the nodes of *Tmem107*^{null} embryos maintain their motile and sensory identities, but the pattern of *Dand5* and *Nodal* expression at the node hint that the leftward flow, or its detection, is compromised. Work in zebrafish has shown that shorter cilia in the Kupffer's vesicle generate slower flow, which results in a failure to degrade *Dand5*, and leads to randomized *Nodal* (Lopes et al., 2010; Sampaio et al., 2014). This phenotype is nearly identical to the phenotype in *Tmem107*^{null} nodes, leading us to believe that although cilia with motile identity are present in *Tmem107*^{null} embryos, the leftward flow is likely not strong enough to result in degradation of *Dand5* on the left side of the node. We do note that among *Tmem107*^{null} embryos with bilateral *Nodal* expression in the LPM, 6/8 have broader expression on the left side. This phenotype may indicate that the flow in *Tmem107*^{null} embryos is predominantly leftward, albeit weak, and *Nodal* becomes initially activated in the left LPM, with its later induction in the right LPM, where it propagates posteriorly (Nakamura et al., 2012). In comparison, cilia numbers in *Tmem107*^{schlei} embryo nodes are similar to control, with overall normal cilia length, presumably resulting in the normal leftward flow, as evidenced by proper L-R patterning in these mutants.

After initiating the L-R patterning process, cells from the node contribute to the notochordal plate (Brennan et al., 2002; Lee and Anderson, 2008; Sulik et al., 1994). Discrepancy in cilia numbers in the nodes of the two *Tmem107* mutants demonstrates another key difference between them - the absence of cilia in the *Tmem107*^{null} midline, and their presence in *Tmem107*^{schlei} (Fig. 7 G). Thus, *Tmem107*^{null} and *Tmem107*^{schlei} mutants represent an

allelic series, and provide us with a unique opportunity to address the requirement for cilia in the node and the midline for the establishment and maintenance of L-R asymmetry.

3.3. Roles for cilia in establishing and maintaining the midline barrier

Cilia are hubs for SHH signaling in mammals and SHH is necessary for the proper formation of the notochord and the floor plate (Chiang et al., 1996). Since *Lefty1* is expressed in the prospective floor plate, we expected its expression to be dependent on presence of cilia and SHH signaling (Tsiairis and McMahon, 2009; Tsukui et al., 1999). Both *Tmem107* mutants show a strong reduction of *FoxA2* in their midlines, suggesting defective SHH signaling, but *Lefty1* is present in the midlines of $Tmm107^{schle}$ (Fig. 7 G). Lack of *Lefty1* in the *Shh* and *FoxA2* mutant mice is likely due to structural defects and lack of the floor plate, rather than the failure to induce its expression through the SHH signaling cascade (Ang and Rossant, 1994; Dufort et al., 1998; Tsukui et al., 1999; Weinstein et al., 1994). Since the floor plate is formed in both $Tmem107^{null}$ and $Tmem107^{schlei}$ mutants, an alternative explanation is that low residual SHH signaling in $Tmem107^{schlei}$ mutant is sufficient for *Lefty1* expression (Christopher et al., 2012).

Loss of normal SHH signaling in the $Tmem107^{schlei}$ midline still allows for the formation of the midline barrier. Therefore, we propose a novel SHH-independent function for cilia in coordinating *Lefty1* expression and establishing the midline barrier. Furthermore, while cilia in the node are required for the establishment of the asymmetry, the midline cilia may be required for the establishment of the midline barrier and maintenance of L-R asymmetry. Thus, our interpretation of the experiments that reintroduce cilia in the crown cells of the node is that full recovery is achieved due to the migration of ciliated cells from the node into the midline, as previously observed in wild-type embryos (Botilde et al., 2013; Brennan et al., 2002; Sulik et al., 1994; Yoshiba et al., 2012).

3.4. Cilia in L-R patterning beyond the node and the midline

Hedgehog signaling has also been implicated in relaying the *Nodal* signal to the LPM (Tsiairis and McMahon, 2009). The model proposes that in Smo^{null} animals *Nodal* is lost from the LPM due to an overactive GLI3 repressor (GLI3R). Consistently, $Smo^{null}; Gli3^{null}$ animals have normal L-R patterning. Furthermore, by introducing *Smo* back into the LPM of Smo^{null} animals, authors show that given proper signaling in the LPM, midline SHH signaling may be dispensable (Tsiairis and McMahon, 2009). Our results are largely in agreement with this model. In $Tmem107^{null}$ animals, the phenotype is akin to loss of cilia, likely inhibiting Gli3R formation, thus making the LPM hypersensitive to NODAL. With the loss of cilia, SHH signaling and *Lefty1* in the midline, NODAL is free to autoactivate in the LPM on both sides. Likewise, $Tmem107^{schlei}$ embryos lack cilia in the LPM, disrupting SHH signaling in that region. However, the presence of cilia, *Lefty1* and a functional midline barrier overcome the potential hypersensitivity to NODAL in $Tmem107^{schlei}$ embryos.

Our genetic interaction experiment with *Tmem107* and *Pkd2* did not yield a clear answer of whether the remaining crown cilia in $Tmem107^{null}$ embryos are functional. However, it does contribute insight towards the investigation of ciliary functions beyond the node. $Pkd2^{null};$

Tmem107^{null} animals present with a left pulmonary isomerism phenotype, like the single *Tmem107*^{null} animals. This phenotype is also similar to *Pkd2*^{null}*; Kif3a*^{null} animals, which lack all cilia, and have been reported to have bilateral *Pitx2* expression, a molecular precursor to left pulmonary isomerism (Grimes et al., 2016). Furthermore, bilateral expression of *Nodal* is also the prevailing phenotype observed in mutants with a complete loss of cilia (Murcia et al., 2000; Takeda et al., 1999). Given all of this evidence, *Tmem107*^{null} appears to behave as a loss of cilia mutant. However, some ciliary functionality is maintained in the embryo, since the mutants in our study survive until at least E16.5, while mutants with a complete loss of cilia, like *Kif3a* and *IFT88* die before E11.5 (Murcia et al., 2000; Takeda et al., 1999).

The experiment with the *Pkd2*^{null}*; Tmem107*^{null} animals advances our understanding for the roles of cilia in the LPM and the midline. Models predict that LPM on both sides may be receiving the NODAL signal at the onset of leftward nodal flow (Nakamura et al., 2006). It has been proposed that cilia may provide an inhibitory signal (like GLI3R) to the propagation of NODAL in the LPM, and the role for PC2 may be to induce signaling that would alleviate that inhibition (Grimes et al., 2016; Tsiairis and McMahon, 2009). Our results agree with this interpretation of the mutant phenotypes, with one caveat. Crown cilia were proposed as the most important contributors in this inhibition/release of inhibition signaling (Grimes et al., 2016), but our data go against this notion, since we found no abnormalities in specification of crown cilia and their ciliary localization of PC2. Instead, it may be a combinatorial mechanism, with the crown cells travelling into the midline, and the midline cilia and the midline barrier playing indispensable role in limiting hyperactivation of NODAL sensitivity in the LPM.

4. Summary

Several mouse mutants of transition zone proteins have been reported to have various L-R patterning defects, including left isomerism or bilateral expression of “leftness” markers in mouse mutants of *Tmem67, Mks1* and *Rpgrip1L* (Abdelhamed et al., 2015; Christopher et al., 2012; Vierkotten et al., 2007; Weatherbee et al., 2009). While some investigation has been carried out into uncovering the mechanism behind left isomerism in mutants lacking cilia, less is known about mutants with a partial loss of cilia. Mouse mutants of transition zone proteins typically have some cilia, albeit with defective ciliary protein composition (Christopher et al., 2012; Dowdle et al., 2011; Roberson et al., 2015; Shylo et al., 2016; Weatherbee et al., 2009). Our finding here that *Tmem107*^{null} animals have left pulmonary isomerism is consistent with the fact that cilia are ubiquitous organelles, and a transition zone is required for the formation of a functional cilium. Although at early stages *Nodal* is randomized at the node in *Tmem107*^{null}, the failure of the midline barrier allows NODAL to cross the midline and induce its expression in the opposite LPM, always leading to its bilateral activation at later stages, and subsequent left isomerism. *Tmem107*^{schlei} animals, on the other hand, provide us with a natural conditional-like mutant, where complete loss of cilia occurs only in the LPM, and the cilia in the nodes and the midline look normal, resulting in normal L-R patterning.

The two mouse mutants for ciliary transition zone protein TMEM107 presented here can be invaluable assets in studying the detailed roles of cilia in establishing L-R asymmetry, and may help address questions about differential requirements for ciliary proteins in different tissues, despite the ubiquitous nature of this organelle. Our data also hint at the potential roles for cilia in establishing and maintaining L-R asymmetry outside the node, consistent with observations made by others (Grimes et al., 2016; Tsiairis and McMahon, 2009).

5. Materials and methods

5.1. Mouse strains

Mouse experiments were performed in accordance with Yale Institutional Animal Care and Use Committee guidelines. The *Tmem107*^{tm1Lex} mouse line, herein referred to as *Tmem107*^{null}, has been previously described (Christopher et al., 2012; Tang et al., 2010). The mouse line was initially generated on the C57BL/6N background, and the analysis in this paper has been performed on a mixed C57BL/6J; C57BL/6N background. *Tmem107*^{schlei} (Christopher et al., 2012) mutant line was crossed for at least 7 generations onto the C57BL/6J background prior to characterization. *Dnah11*^{GFP} (*Lrd*^{GFP}) (McGrath et al., 2003) mice were a gift of Martina Brueckner, and are maintained on a mixed genetic background of unknown composition. *Pkd2*^{tm2Som} mice (Wu et al., 1998) are maintained on a mixed genetic background of unknown composition. Genotyping primers and strategies are available in Supplementary Material, Table S1.

Timed matings were set up by pairing up male and female mice in the evenings. The following morning females were checked for the presence of vaginal plugs. If a plug was detected, noon on that day was designated embryonic day E0.5. Females were euthanized, and embryos were collected at E8.0-E16.5. Embryos were staged morphologically as E8.0 starting at the late head fold, and as E8.5 once they had 6 somites, and the heart had begun to loop.

5.2. Expression analysis

In situ hybridization analyses were performed using standard methods (Nagy, 2003). Embryos were collected in sterile PBS, and yolk sac was used for genotyping. Mutant and control embryos of appropriate stages were pooled from multiple litters into corresponding groups. The two groups were treated identically throughout the protocol. The timing to stop the alkaline phosphatase reaction was empirically determined, but was identical for mutant and control embryos in the same experiment.

Antisense probes were generated from the following cDNA plasmids: *Nodal* (Elizabeth Robertson), *Dand5* (Martina Brueckner), *Lefty1* (Hiroshi Hamada), *Pitx2* (Axel Schweickart), *Ptch1, Shh* and *FoxA2* (Andrew McMahon).

The *Tmem107* riboprobe plasmid was generated by RT-PCR from C57BL/6J RNA with subsequent cloning into pCRII-TOPO and contains full-length mouse *Tmem107* (NM_025838.2) coding sequence. *In situ* hybridization with *Tmem107* sense probe showed no visible staining (not shown).

5.3. Wholemount immunostaining

Embryos were collected at E8.0-E8.5 and fixed in 4% paraformaldehyde (PFA) for 20 min at room temperature. Embryos were washed 3 times (15 min each) in phosphate buffered saline (PBS), then blocked with 1% goat serum and 0.1% Triton-X in PBS (PBGT) for 1 h at room temperature. Primary antibodies in PBGT were added and incubated overnight at 4 °C. After 315 min washes in PBGT, secondary antibodies in PBGT were added for 2 h at room temperature. Then, samples were washed 3 times (15 min each) in PBS and 0.1% Triton-X, and mounted on slides (Denville) using ProLong Diamond Antifade Mountant (Life Technologies). Antibodies used are available in Supplementary Material, Table S2.

Alternatively, embryos previously dehydrated in methanol series were rehydrated, blocked in PBGT, and the protocol was followed as described above.

To acquire sections through the midline, embryos were stained as wholemount and imaged, then rinsed 3 times in PBS and 0.1% Triton-X, dehydrated in 30% sucrose, embedded in OCT and cryosectioned. Coverslips were applied to sections with ProLong Diamond Antifade Mountant.

5.4. Imaging and image analysis

Images of organs and post-*in situ* hybridization embryos were taken on a Zeiss SteREO Discovery microscope. Wholemount immunofluorescence images were captured using Leica SP5 inverted confocal microscope using Leica Application Software. Immunofluorescent images of sectioned embryos were acquired on Carl Zeiss LSM 700 confocal microscope.

Image analysis was performed in ImageJ (NIH). Specifically, cilia were counted using the point tool, and their length was determined using the line tool and known image scale. Optical sections through midlines were acquired using Reslice function, and then a Z-stack projection was created from the region of interest. Resulting images were slightly stretched out in dorsal-ventral direction for easier visualization.

Graphs created and statistical analysis regarding cilia numbers and length were carried out using Prism software.

Supplementary Material

Refer to Web version on PubMed Central for supplementary material.

Acknowledgements

We would like to thank Kasey Christopher for the original observation of left-right patterning defects in *Tmem107*^{null} animals; Martina Brueckner and Karel Liem for continued support of this project through sharing resources, as well as constructive discussions of the results and feedback on the manuscript; Davis Li and other members of the Weatherbee and Liem laboratories for feedback on experimental design, and manuscript preparation. Particular thanks go to Emilie League for help with samples and for detailed manuscript feedback. Furthermore, we would like to thank Paul Trainor from Stowers Institute for generous resources, support and feedback in the final stages of manuscript preparation. This manuscript is partially based on a dissertation submitted to fulfill in part the requirements for the degree of Doctor of Philosophy, Yale University.

Funding

This publication was made possible by grant R01HD093608 from the National Institute of Child Health and Human Development, P30DK090744 from the National Institute of Diabetes and Digestive and Kidney Diseases and N.A.S. was supported by National Institute of General Medical Sciences training grant T32GM007499 and National Science Foundation Gradate Research Fellowship Grant DGE-1122492.

References

Abdelhamed ZA, Natarajan S, Wheway G, Inglehearn CF, Toomes C, Johnson CA, Jagger DJ, 2015 The Meckel-Gruber syndrome protein TMEM67 controls basal body positioning and epithelial branching morphogenesis in mice via the non-canonical Wnt pathway. Dis. Models Mech 8, 527–541.

Ang SL, Rossant J, 1994 HNF-3 beta is essential for node and notochord formation in mouse development. Cell 78, 561–574. [PubMed: 8069909]

Botilde Y, Yoshiba S, Shinohara K, Hasegawa T, Nishimura H, Shiratori H, Hamada H, 2013 Cluap1 localizes preferentially to the base and tip of cilia and is required for ciliogenesis in the mouse embryo. Dev. Biol 381, 203–212. [PubMed: 23742838]

Brennan J, Norris DP, Robertson EJ, 2002 Nodal activity in the node governs left-right asymmetry. Genes Dev. 16, 2339–2344. [PubMed: 12231623]

Cai Y, Maeda Y, Cedzich A, Torres V, Wu G, Tomohito H, Toshio M, Jong Hoon P, Ralph W, Stefan S, 1999 Identification and characterization of polycystin-2, the PKD2 gene product. J. Biol. Chem 274, 28557–28565. [PubMed: 10497221]

Caspary T, Larkins C, Anderson K, 2007 The graded response to Sonic Hedgehog depends on cilia architecture. Dev. Cell 12, 767–778. [PubMed: 17488627]

Chiang C, Litingtung Y, Lee E, Young KE, Corden JL, Westphal H, Beachy PA, 1996 Cyclopia and defective axial patterning in mice lacking Sonic hedgehog gene function. Nature 383, 407–413. [PubMed: 8837770]

Christopher KJ, Wang B, Kong Y, Weatherbee SD, 2012 Forward genetics uncovers Transmembrane protein 107 as a novel factor required for ciliogenesis and Sonic hedgehog signaling. Dev. Biol 368, 382–392. [PubMed: 22698544]

Cui C, Chatterjee B, Francis D, Yu Q, SanAgustin JT, Francis R, Tansey T, Henry C, Wang B, Lemley B, et al., 2011 Disruption of Mks1 localization to the mother centriole causes cilia defects and developmental malformations in Meckel-Gruber syndrome. Dis. Models Mech 4, 43–56.

Diez-Roux G, Banfi S, Sultan M, Geffers L, Anand S, Rozado D, Magen A, Canidio E, Pagani M, Peluso I, et al., 2011 A high-resolution anatomical atlas of the transcriptome in the mouse embryo. PLoS Biol. 9, e1000582. [PubMed: 21267068]

Dougherty GW, Loges NT, Klinkenbusch JA, Olbrich H, Pennekamp P, Menchen T, Raidt J, Wallmeier J, Werner C, Westermann C, et al., 2016 DNAH11 localization in the proximal region of respiratory cilia defines distinct outer dynein arm complexes. Am. J. Respir. Cell Mol. Biol 55, 213–224. [PubMed: 26909801]

Dowdle WE, Robinson JF, Kneist A, Sirerol-Piquer MS, Frints SG, Corbit KC, Zaghloul NA, van Lijnschoten G, Mulders L, Verver DE, et al., 2011 Disruption of a ciliary B9 protein complex causes Meckel syndrome. Am. J. Hum. Genet 89, 94–110. [PubMed: 21763481]

Dufort D, Schwartz L, Harpal K, Rossant J, 1998 The transcription factor HNF3beta is required in visceral endoderm for normal primitive streak morphogenesis. Development 125, 3015–3025. [PubMed: 9671576]

Echelard Y, Epstein DJ, St-Jacques B, Shen L, Mohler J, McMahon JA, McMahon AP, 1993 Sonic hedgehog, a member of a family of putative signaling molecules, is implicated in the regulation of CNS polarity. Cell 75, 1417–1430. [PubMed: 7916661]

Garcia-Gonzalo FR, Corbit KC, Sirerol-Piquer MS, Ramaswami G, Otto EA, Noriega TR, Seol AD, Robinson JF, Bennett CL, Josifova DJ, et al., 2011 A transition zone complex regulates mammalian ciliogenesis and ciliary membrane composition. Nat. Genet 43, 776–784. [PubMed: 21725307]

Garcia-Gonzalo FR, Reiter JF, 2017 Open sesame: how transition fibers and the transition zone control ciliary composition. Cold Spring Harb. Perspect. Biol 9.

Grimes DT, Keynton JL, Buenavista MT, Jin X, Patel SH, Kyosuke S, Vibert J, Williams DJ, Hamada H, Hussain R, et al., 2016 Genetic analysis reveals a hierarchy of interactions between polycystin-encoding genes and genes controlling cilia function during left-right determination. PLoS Genet. 12, e1006070. [PubMed: 27272319]

Harris PC, Rossetti S, 2010 Determinants of renal disease variability in ADPKD. Adv. Chron. Kidney Dis 17, 131–139.

Hashimoto M, Shinohara K, Wang J, Ikeuchi S, Yoshiba S, Meno C, Nonaka S, Takada S, Hatta K, Wynshaw-Boris A, et al., 2010 Planar polarization of node cells determines the rotational axis of node cilia. Nat. Cell Biol 12, 170–176. [PubMed: 20098415]

Huangfu D, Liu A, Rakeman AS, Murcia NS, Niswander L, Anderson KV, 2003 Hedgehog signalling in the mouse requires intraflagellar transport proteins. Nature 426, 83–87. [PubMed: 14603322]

Inacio JM, Marques S, Nakamura T, Shinohara K, Meno C, Hamada H, Belo JA, 2013 The dynamic right-to-left translocation of Cerl2 is involved in the regulation and termination of Nodal activity in the mouse node. PLoS One 8, e60406. [PubMed: 23544137]

Ishimura A, Chida S, Osada S, 2008 Man1, an inner nuclear membrane protein, regulates left-right axis formation by controlling nodal signaling in a node-independent manner. Dev. Dynam. : Off. Publ. Am. Assoc. Anat 237, 3565–3576.

Kawasumi A, Nakamura T, Iwai N, Yashiro K, Saijoh Y, Belo JA, Shiratori H, Hamada H, 2011 Left-right asymmetry in the level of active Nodal protein produced in the node is translated into left-right asymmetry in the lateral plate of mouse embryos. Dev. Biol 353, 321–330. [PubMed: 21419113]

Kim SJ, 2011 Heterotaxy syndrome. Korean Circ. J 41, 227–232. [PubMed: 21731561]

Lambacher NJ, Bruel AL, van Dam TJ, Szymanska K, Slaats GG, Kuhns S, McManus GJ, Kennedy JE, Gaff K, Wu KM, et al., 2016 TMEM107 recruits ciliopathy proteins to subdomains of the ciliary transition zone and causes Joubert syndrome. Nat. Cell Biol 18, 122–131. [PubMed: 26595381]

Layton WM Jr., 1976 Random determination of a developmental process: reversal of normal visceral asymmetry in the mouse. J. Hered 67, 336–338. [PubMed: 1021593]

Lee JD, Anderson KV, 2008 Morphogenesis of the node and notochord: the cellular basis for the establishment and maintenance of left-right asymmetry in the mouse. Dev. Dynam. : Off. Publ. Am. Assoc. Anat 237, 3464–3476.

Li Y, Klena NT, Gabriel GC, Liu X, Kim AJ, Lemke K, Chen Y, Chatterjee B, Devine W, Damerla RR, et al., 2015 Global genetic analysis in mice unveils central role for cilia in congenital heart disease. Nature 521, 520–524. [PubMed: 25807483]

Lin AE, Krikov S, Riehle-Colarusso T, Frias JL, Belmont J, Anderka M, Geva T, Getz KD, Botto LD, National Birth Defects Prevention, S., 2014 Laterality defects in the national birth defects prevention study (1998–2007): birth prevalence and descriptive epidemiology. Am. J. Med. Genet 164A, 2581–2591. [PubMed: 25099286]

Lin CR, Kioussi C, O'Connell S, Briata P, Szeto D, Liu F, Izpisua-Belmonte JC, Rosenfeld MG, 1999 Pitx2 regulates lung asymmetry, cardiac positioning and pituitary and tooth morphogenesis. Nature 401, 279–282. [PubMed: 10499586]

Lopes SS, Lourenco R, Pacheco L, Moreno N, Kreiling J, Saude L, 2010 Notch signalling regulates left-right asymmetry through ciliary length control. Development 137, 3625–3632. [PubMed: 20876649]

Mahaffey JP, Grego-Bessa J, Liem KF Jr., Anderson KV, 2013 Cofilin and Vangl2 cooperate in the initiation of planar cell polarity in the mouse embryo. Development 140, 1262–1271. [PubMed: 23406901]

Marques S, Borges AC, Silva AC, Freitas S, Cordenonsi M, Belo JA, 2004 The activity of the Nodal antagonist Cerl-2 in the mouse node is required for correct L/R body axis. Genes Dev. 18, 2342–2347. [PubMed: 15466485]

May-Simera HL, Kai M, Hernandez V, Osborn DP, Tada M, Beales PL, 2010 Bbs8, together with the planar cell polarity protein Vangl2, is required to establish left-right asymmetry in zebrafish. Dev. Biol 345, 215–225. [PubMed: 20643117]

McGrath J, Somlo S, Makova S, Tian X, Brueckner M, 2003 Two populations of node monocilia initiate left-right asymmetry in the mouse. Cell 114, 61–73. [PubMed: 12859898]

Meno C, Ito Y, Saijoh Y, Matsuda Y, Tashiro K, Kuhara S, Hamada H, 1997 Two closely-related left-right asymmetrically expressed genes, lefty-1 and lefty-2: their distinct expression domains, chromosomal linkage and direct neuralizing activity in Xenopus embryos. Genes Cells : Devoted Mol. Cell. Mech 2, 513–524.

Meno C, Shimono A, Saijoh Y, Yashiro K, Mochida K, Ohishi S, Noji S, Kondoh H, Hamada H, 1998 lefty-1 is required for left-right determination as a regulator of lefty-2 and nodal. Cell 94, 287–297. [PubMed: 9708731]

Metzger RJ, Klein OD, Martin GR, Krasnow MA, 2008 The branching programme of mouse lung development. Nature 453, 745–750. [PubMed: 18463632]

Murcia NS, Richards WG, Yoder BK, Mucenski ML, Dunlap JR, Woychik RP, 2000 The Oak Ridge Polycystic Kidney (orpk) disease gene is required for left-right axis determination. Development 127, 2347–2355. [PubMed: 10804177]

Nagy A, 2003 In: Manipulating the Mouse Embryo : a Laboratory Manual, third ed. Cold Spring Harbor Laboratory Press, Cold Spring Harbor, N.Y.

Nakamura T, Mine N, Nakaguchi E, Mochizuki A, Yamamoto M, Yashiro K, Meno C, Hamada H, 2006 Generation of robust left-right asymmetry in the mouse embryo requires a self-enhancement and lateral-inhibition system. Dev. Cell 11, 495–504. [PubMed: 17011489]

Nakamura T, Saito D, Kawasumi A, Shinohara K, Asai Y, Takaoka K, Dong F, Takamatsu A, Belo JA, Mochizuki A, et al., 2012 Fluid flow and interlinked feedback loops establish left-right asymmetric decay of Cerl2 mRNA. Nat. Commun 3, 1322. [PubMed: 23271656]

Nonaka S, Yoshiba S, Watanabe D, Ikeuchi S, Goto T, Marshall WF, Hamada H, 2005 De novo formation of left-right asymmetry by posterior tilt of nodal cilia. PLoS Biol. 3, e268. [PubMed: 16035921]

Norris DP, Brennan J, Bikoff EK, Robertson EJ, 2002 The Foxh1-dependent autoregulatory enhancer controls the level of Nodal signals in the mouse embryo. Development 129, 3455–3468. [PubMed: 12091315]

Norris DP, Grimes DT, 2012 Mouse models of ciliopathies: the state of the art. Dis. Models Mech 5, 299–312.

Pennekamp P, Karcher C, Fischer A, Schweickert A, Skryabin B, Horst J, Blum M, Dworniczak B, 2002 The ion channel polycystin-2 is required for left-right axis determination in mice. Curr. Biol. : CB 12, 938–943. [PubMed: 12062060]

Pennekamp P, Menchen T, Dworniczak B, Hamada H, 2015 Situs inversus and ciliary abnormalities: 20 years later, what is the connection? Cilia 4, 1. [PubMed: 25589952]

Piedra ME, Icardo JM, Albajar M, Rodriguez-Rey JC, Ros MA, 1998 Pitx2 participates in the late phase of the pathway controlling left-right asymmetry. Cell 94, 319–324. [PubMed: 9708734]

Roberson EC, Dowdle WE, Ozanturk A, Garcia-Gonzalo FR, Li C, Halbritter J, Elkhartoufi N, Porath JD, Cope H, Ashley-Koch A, et al., 2015 TMEM231, mutated in orofaciodigital and Meckel syndromes, organizes the ciliary transition zone. J. Cell Biol 209, 129–142. [PubMed: 25869670]

Ryan AK, Blumberg B, Rodriguez-Esteban C, Yonei-Tamura S, Tamura K, Tsukui T, de la Pena J, Sabbagh W, Greenwald J, Choe S, et al., 1998 Pitx2 determines left-right asymmetry of internal organs in vertebrates. Nature 394, 545–551. [PubMed: 9707115]

Sampaio P, Ferreira RR, Guerrero A, Pintado P, Tavares B, Amaro J, Smith AA, Montenegro-Johnson T, Smith DJ, Lopes SS, 2014 Left-right organizer flow dynamics: how much cilia activity reliably yields laterality? Dev. Cell 29, 716–728. [PubMed: 24930722]

Schweickert A, Vick P, Getwan M, Weber T, Schneider I, Eberhardt M, Beyer T, Pachur A, Blum M, 2010 The nodal inhibitor Coco is a critical target of leftward flow in Xenopus. Curr. Biol. : CB 20, 738–743. [PubMed: 20381352]

Seo JW, Brown NA, Ho SY, Anderson RH, 1992 Abnormal laterality and congenital cardiac anomalies. Relations of visceral and cardiac morphologies in the iv/iv mouse. Circulation 86, 642–650. [PubMed: 1638728]

Shaheen R, Almoisheer A, Faqeih E, Babay Z, Monies D, Tassan N, Abouelhoda M, Kurdi W, Al Mardawi E, Khalil MM, et al., 2015 Identification of a novel MKS locus defined by TMEM107 mutation. Hum. Mol. Genet 24, 5211–5218. [PubMed: 26123494]

Shaheen R, Faqeih E, Alshammari MJ, Swaid A, Al-Gazali L, Mardawi E, Ansari S, Sogaty S, Seidahmed MZ, AlMotairi MI, et al., 2013 Genomic analysis of Meckel-Gruber syndrome in Arabs reveals marked genetic heterogeneity and novel candidate genes. Eur. J. Hum. Genet. : EJHG (Eur. J. Hum. Genet.) 21, 762–768. [PubMed: 23169490]

Shinohara K, Kawasumi A, Takamatsu A, Yoshiba S, Botilde Y, Motoyama N, Reith W, Durand B, Shiratori H, Hamada H, 2012 Two rotating cilia in the node cavity are sufficient to break left-right symmetry in the mouse embryo. Nat. Commun 3, 622. [PubMed: 22233632]

Shylo NA, Christopher KJ, Iglesias A, Daluiski A, Weatherbee SD, 2016 TMEM107 is a critical regulator of ciliary protein composition and is mutated in orofaciodigital syndrome. Hum. Mutat 37, 155–159. [PubMed: 26518474]

Song H, Hu J, Chen W, Elliott G, Andre P, Gao B, Yang Y, 2010 Planar cell polarity breaks bilateral symmetry by controlling ciliary positioning. Nature 466, 378–382. [PubMed: 20562861]

Sulik K, Dehart DB, Iangaki T, Carson JL, Vrablic T, Gesteland K, Schoenwolf GC, 1994 Morphogenesis of the murine node and notochordal plate. Dev. Dynam. : Off. Publ. Am. Assoc. Anat 201, 260–278.

Supp DM, Witte DP, Potter SS, Brueckner M, 1997 Mutation of an axonemal dynein affects left-right asymmetry in inversus viscerum mice. Nature 389, 963–966. [PubMed: 9353118]

Szymanska K, Johnson CA, 2012 The transition zone: an essential functional compartment of cilia. Cilia 1, 10. [PubMed: 23352055]

Takeda S, Yonekawa Y, Tanaka Y, Okada Y, Nonaka S, Hirokawa N, 1999 Left-right asymmetry and kinesin superfamily protein KIF3A: new insights in determination of laterality and mesoderm induction by kif3A−/− mice analysis. J. Cell Biol 145, 825–836. [PubMed: 10330409]

Tang T, Li L, Tang J, Li Y, Lin WY, Martin F, Grant D, Solloway M, Parker L, Ye W, et al., 2010 A mouse knockout library for secreted and transmembrane proteins. Nat. Biotechnol 28, 749–755. [PubMed: 20562862]

Tsiairis CD, McMahon AP, 2009 An Hh-dependent pathway in lateral plate mesoderm enables the generation of left/right asymmetry. Curr. Biol. : CB 19, 1912–1917. [PubMed: 19879143]

Tsukui T, Capdevila J, Tamura K, Ruiz-Lozano P, Rodriguez-Esteban C, Yonei-Tamura S, Magallon J, Chandraratna RA, Chien K, Blumberg B, et al., 1999 Multiple left-right asymmetry defects in Shh(−/−) mutant mice unveil a convergence of the shh and retinoic acid pathways in the control of Lefty-1. Proc. Natl. Acad. Sci. U. S. A 96, 11376–11381. [PubMed: 10500184]

Vierkotten J, Dildrop R, Peters T, Wang B, Ruther U, 2007 Ftm is a novel basal body protein of cilia involved in Shh signalling. Development 134, 2569–2577. [PubMed: 17553904]

Weatherbee SD, Niswander LA, Anderson KV, 2009 A mouse model for Meckel syndrome reveals Mks1 is required for ciliogenesis and Hedgehog signaling. Hum. Mol. Genet 18, 4565–4575. [PubMed: 19776033]

Weinstein DC, Ruiz i Altaba A, Chen WS, Hoodless P, Prezioso VR, Jessell TM, Darnell JE Jr., 1994 The winged-helix transcription factor HNF-3 beta is required for notochord development in the mouse embryo. Cell 78, 575–588. [PubMed: 8069910]

Wu G, D'Agati V, Cai Y, Markowitz G, Park JH, Reynolds DM, Maeda Y, Le TC, Hou H Jr., Kucherlapati R, et al., 1998 Somatic inactivation of Pkd2 results in polycystic kidney disease. Cell 93, 177–188. [PubMed: 9568711]

Yamamoto M, Mine N, Mochida K, Sakai Y, Saijoh Y, Meno C, Hamada H, 2003 Nodal signaling induces the midline barrier by activating Nodal expression in the lateral plate. Development 130, 1795–1804. [PubMed: 12642485]

Yang TT, Su J, Wang WJ, Craige B, Witman GB, Tsou MF, Liao JC, 2015 Superresolution pattern recognition reveals the architectural map of the ciliary transition zone. Sci. Rep 5, 14096. [PubMed: 26365165]

Yoshiba S, Shiratori H, Kuo IY, Kawasumi A, Shinohara K, Nonaka S, Asai Y, Sasaki G, Belo JA, Sasaki H, et al., 2012 Cilia at the node of mouse embryos sense fluid flow for left-right determination via Pkd2. Science 338, 226–231. [PubMed: 22983710]

Yoshioka H, Meno C, Koshiba K, Sugihara M, Itoh H, Ishimaru Y, Inoue T, Ohuchi H, Semina EV, Murray JC, et al., 1998 Pitx2, a bicoid-type homeobox gene, is involved in a lefty-signaling pathway in determination of left-right asymmetry. Cell 94, 299–305. [PubMed: 9708732]

Zhang XM, Ramalho-Santos M, McMahon AP, 2001 Smoothened mutants reveal redundant roles for Shh and Ihh signaling including regulation of L/R asymmetry by the mouse node. Cell 105, 781–792. [PubMed: 11440720]

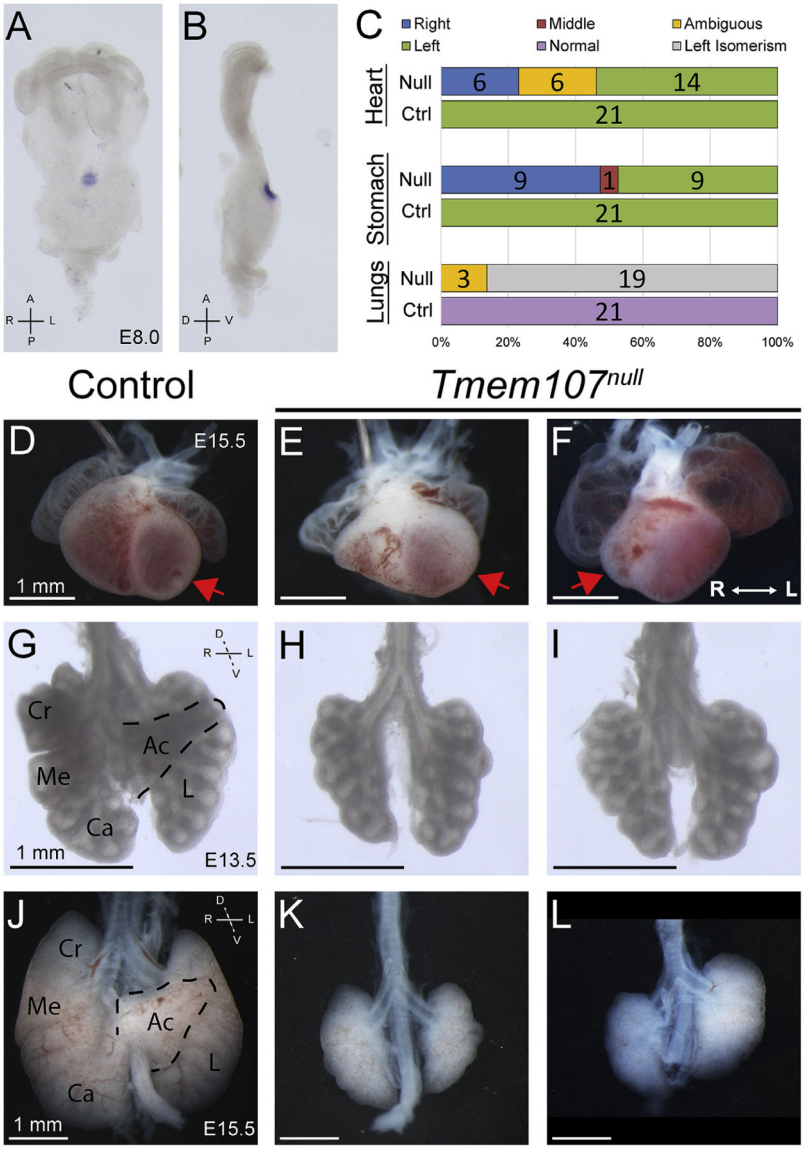

Fig. 1. *Tmem107*^{null} mutants display multiple left-right patterning defects.

(A, B) *Tmem1*07 mRNA is strongly enriched in the nodes of E8.0 embryos, as shown in (A) ventral view and (B) lateral view. (C) Heart positioning (based on the orientation of the apex to the left or right) and stomach positioning are randomized in *Tmem107*^{null} embryos. Mutant lungs predominantly have left isomerism, not observed in control lungs. Numbers represent individual animals. (D–F) Ventral view of E15.5 hearts. Control hearts have their apices on left (D, red arrow), while *Tmem107*^{null} hearts have randomized looping with the apex on left (E, arrow) or right (F, arrow). (G–L) Ventral view of E13.5 (G–I) and E15.5 (J–L) lungs. Control mouse lungs have 4 right lobes and a single left lung lobe, while *Tmem107*^{null} lungs display single lobes on both sides (H, I, K, L), suggesting left pulmonary isomerism. Pulmonary hypoplasia in *Tmem107*^{null} mutants becomes pronounced by E15.5 (K, L). Cr - cranial lobe, Me - medial lobe, Ca - caudal lobe, Ac - accessory lobe, L - left lobe. Scale bars = 1 mm.

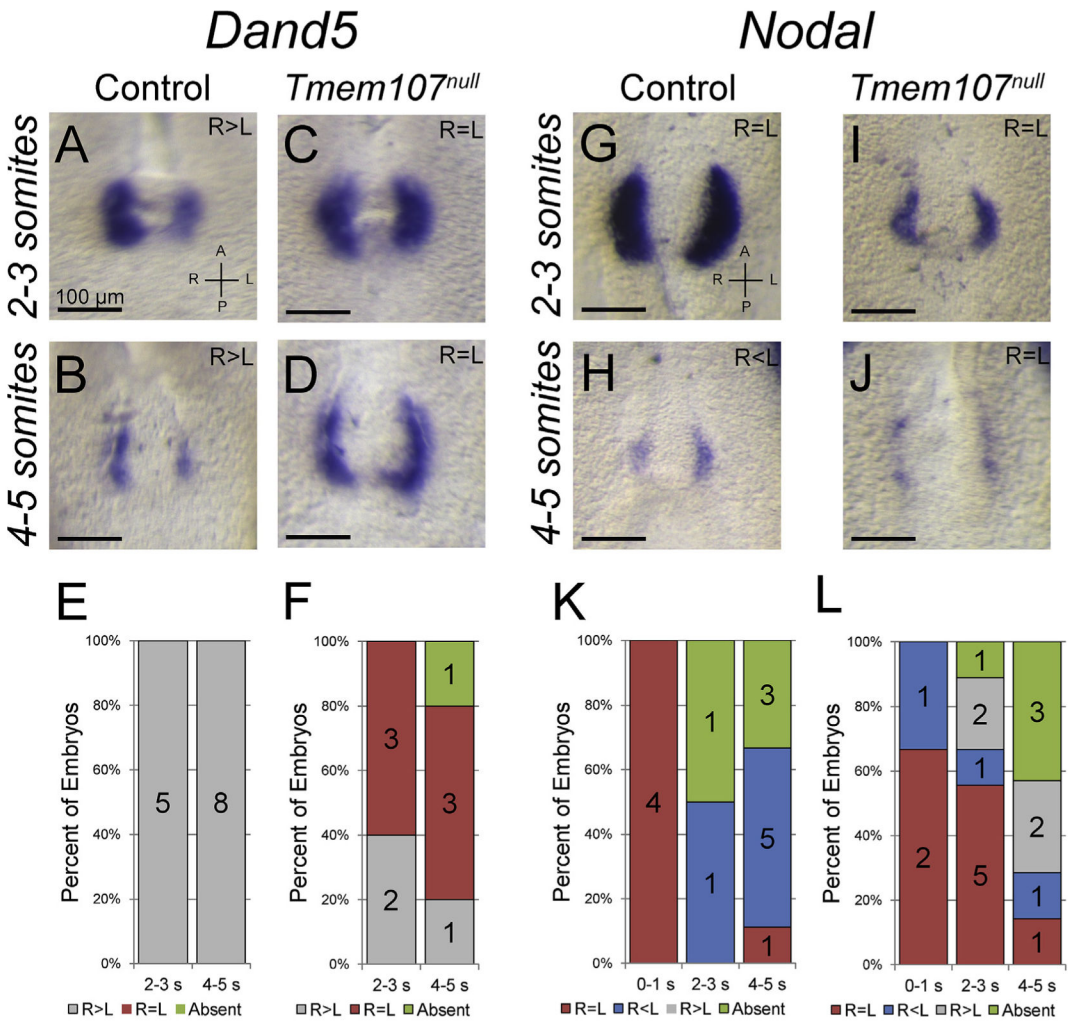

Fig. 2. Flow-induced signaling in *Tmem107*^{null} nodes is compromised.

(A–D) *in situ* hybridization for *Dand5*, at early (2–3 somites) and late (4–5 somites) stages. Control embryos (A, B) show progressive degradation of *Dand5* mRNA on the left side, while *Tmem107*^{null} embryos (C, D) maintain bilateral *Dand5* mRNA, with some randomization of expression at later stages. (G–J) *in situ* hybridization for *Nodal*, at early (2–3 somites) and late (4–5 somites) stages. Control embryos (G, H) show reduced *Nodal* expression on the right side at late stages (H), while *Tmem107*^{null} embryos (I, J) maintain bilateral *Nodal* mRNA for longer, and ultimately have a randomized pattern of expression (L). (E, F, K, L) Graphs accompanying each probe represent the quantification of the embryos with a given expression pattern, broken down by somite number. Scale bars are 100 µm.

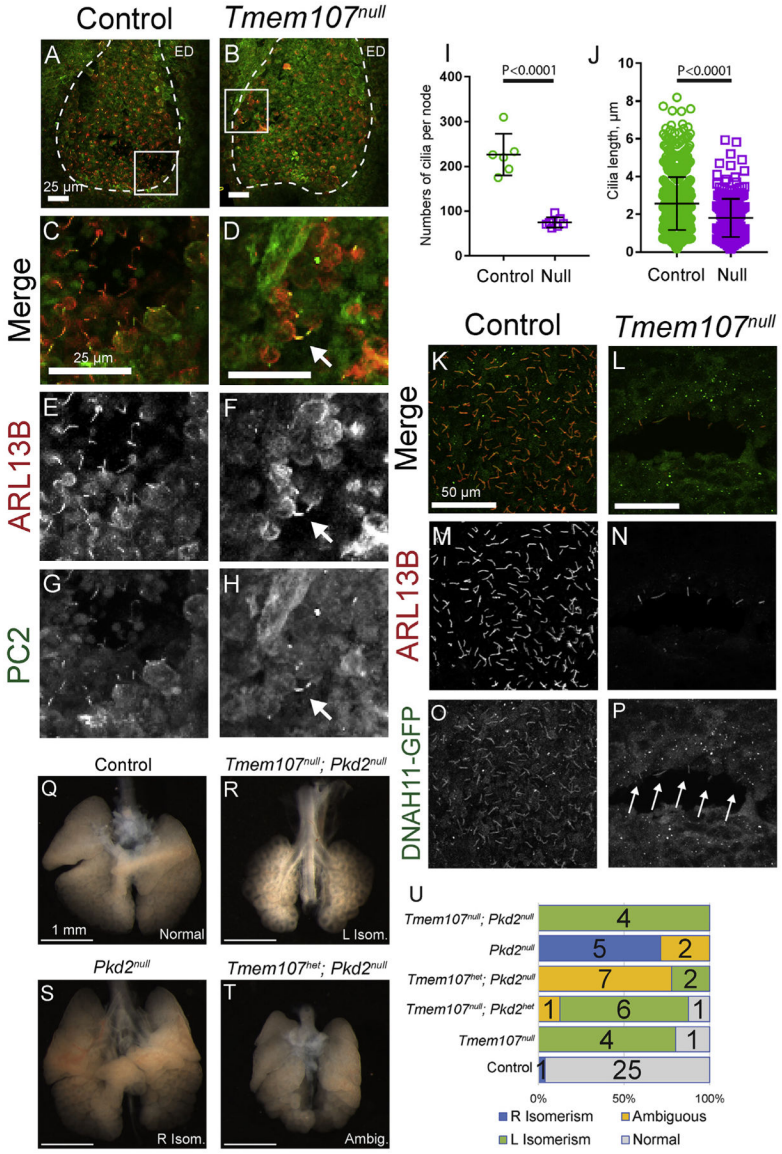

Fig. 3. Motile and sensory cilia are present in *Tmem107*^{null} nodes, but in reduced numbers.

(A-H, K–P) Maximum intensity projected Z-stacks of confocal immunofluorescent images of E8.0 nodes. (A, B) Low magnification images of control (A) and *Tmem107*^{null} (B) nodes show normal cilia numbers in the node and endoderm (ED) in control, but low cilia numbers in *Tmem107*^{null} nodes, and none in ED. (C, D) High magnification images of inserts in A and B, respectively. (C, E) in control, ARL13B (red) is present in all cilia in the node. (D, F) In *Tmem107*^{null} embryos ARL13B is only present in a small population of nodal cilia. (C, G) Polycystin2 (PC2, green) is enriched in sensory cilia on crown cells, around the edge of the node. The distribution of PC2 positive cilia appears normal in *Tmem107*^{null} nodes (B, D, H). (I) Quantification of the cilia in the control (n = 6) and *Tmem107*^{null} (n = 7) nodes show significant loss of cilia in the *Tmem107*^{null} ($P < 0.0001$) (J) Cilia are significantly shorter in *Tmem107*^{null} embryos (n = 285 cilia), compared to control (n = 824 cilia) ($P < 0.001$). (K–P) High magnification views of the nodal pits of control and *Tmem107*^{null} embryos that are

also homozygous for the *Dnah11*^{GFP} transgene. ARL13B (M, N, and red in K, L) marks the nodal cilia showing that the nodal pit of *Tmem107*^{null} embryos has only a small population of ARL13B positive cilia. Control embryos have DNAH11-GFP positive motile cilia (K, green and O) throughout the pit of the node. Cilia in the pit of *Tmem107*^{null} nodes also have motile identity as marked by DNAH11-GFP (L, green and P). (Q–T) Four classes of lung phenotypes observed in this study. (Q) Normal – single lobe on left, four on right. (R) Left isomerism was the dominant phenotype observed in *Tmem107*^{null}*; Pkd2*^{null} animals. (S) many *Pkd2*^{null} animals had right isomerism. (T) Ambiguous lungs phenotype encompasses a range of lungs that have some lobation on either side, but neither left nor right isomerism. Most frequently observed in *Tmem107*^{het}*; Pkd22*^{null} animals. (U) Graphic representation for the quantification of the embryos with a given lung phenotype. Numbers represent individual embryos. ED - endoderm. Scale bars in (A–H) are 25 μm, in (K–P) are 50 μm, and 1 mm in (Q–T). Unpaired *t*-test used for statistical analysis. Error bars represent standard deviation.

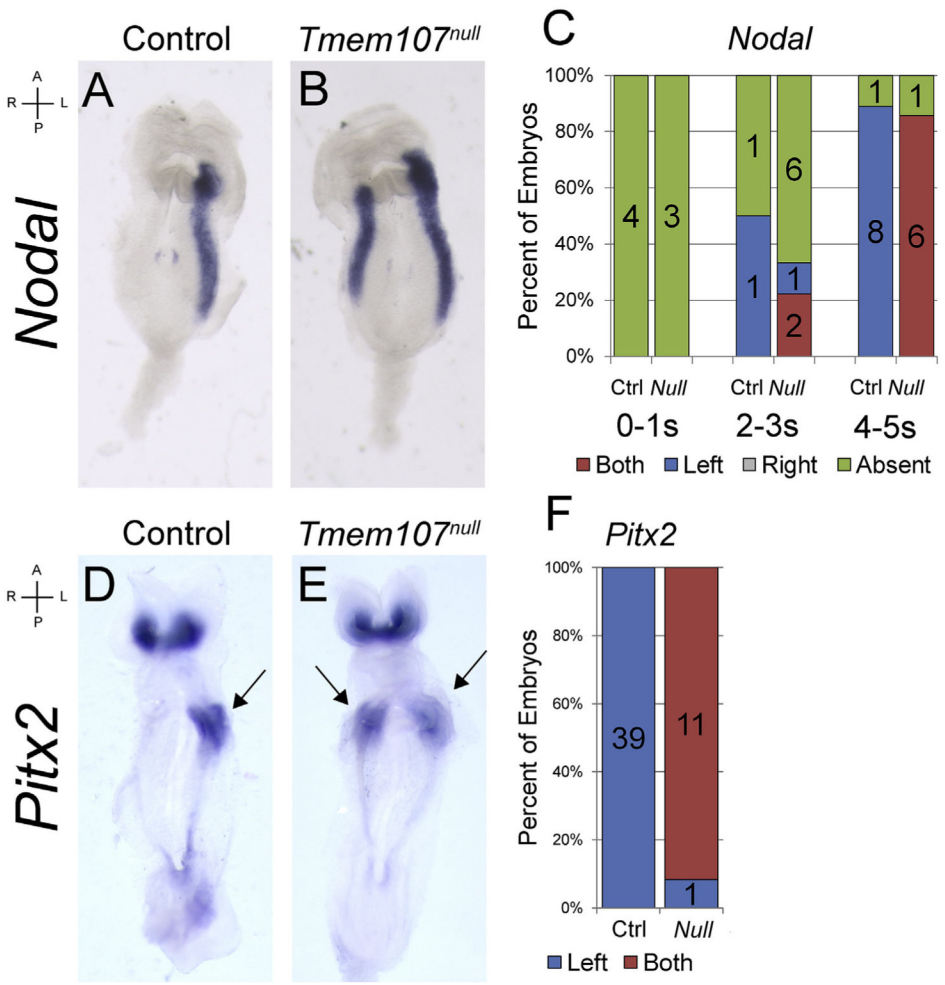

Fig. 4. The lateral plate mesoderm in *Tmem107*^{null} embryos acquires bilateral left identity.

(A, B) *in situ* hybridization for *Nodal* in representative control (A) and *Tmem107*^{null} (B) E8.0 embryos showing left side restriction in controls and bilateral expression in mutants. (C) Quantification of the expression patterns for *Nodal* at the LPM, broken down by somite stage. (D, E) *in situ* hybridization for *Pitx2* in representative control (D, left LPM, arrow) and *Tmem107*^{null} (E, bilateral, arrows) E8.5 embryos. *Pitx2* is normally expressed bilaterally in the developing heads of control and mutant embryos. (F) Quantification of the *Pitx2* expression localization. Numbers in all graphs indicate individual animals.

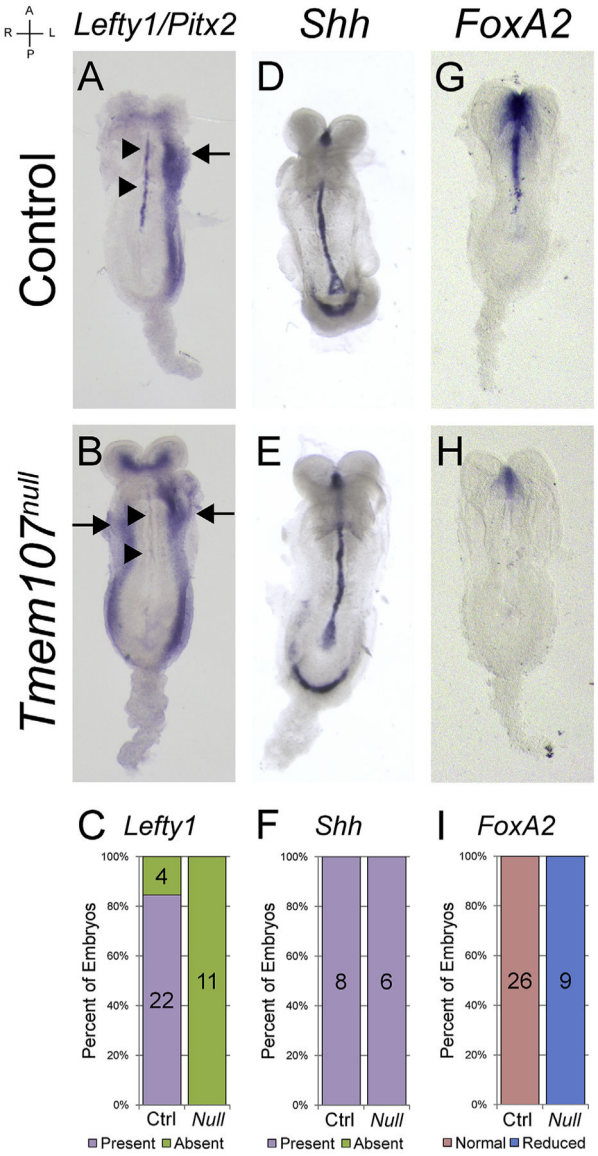

Fig. 5. *Tmem107*^{null} embryos show *Shh*-dependent loss of the midline barrier.

(A, B) Double *in situ* hybridization for *Lefty1* (midline, arrowheads) and *Pitx2* (LPM, arrows) in representative control (A) and *Tmem107*^{null} (B) embryos. *Pitx2* riboprobe was used as a positive control for *in situ* hybridization reaction conditions, and is expressed in left LPM in control embryos (A, arrow) but is bilateral in *Tmem107*^{null} embryos (B, arrows). In contrast, *Lefty1* signal is lost in the midlines of *Tmem107*^{null} embryos (B, arrowheads). (D, E) *in situ* hybridization revealed unchanged midline expression of *Shh* in *Tmem107*^{null} (E) embryos compared to controls (D). (G, H) However, *in situ* hybridization for *FoxA2*, a direct target of SHH signaling, uncovered a strong reduction of midline *FoxA2* expression in *Tmem107*^{null} (H) embryos compared to controls (G). (C, F, I) Graphs accompanying each probe represent the quantification of the embryos with a given expression pattern.

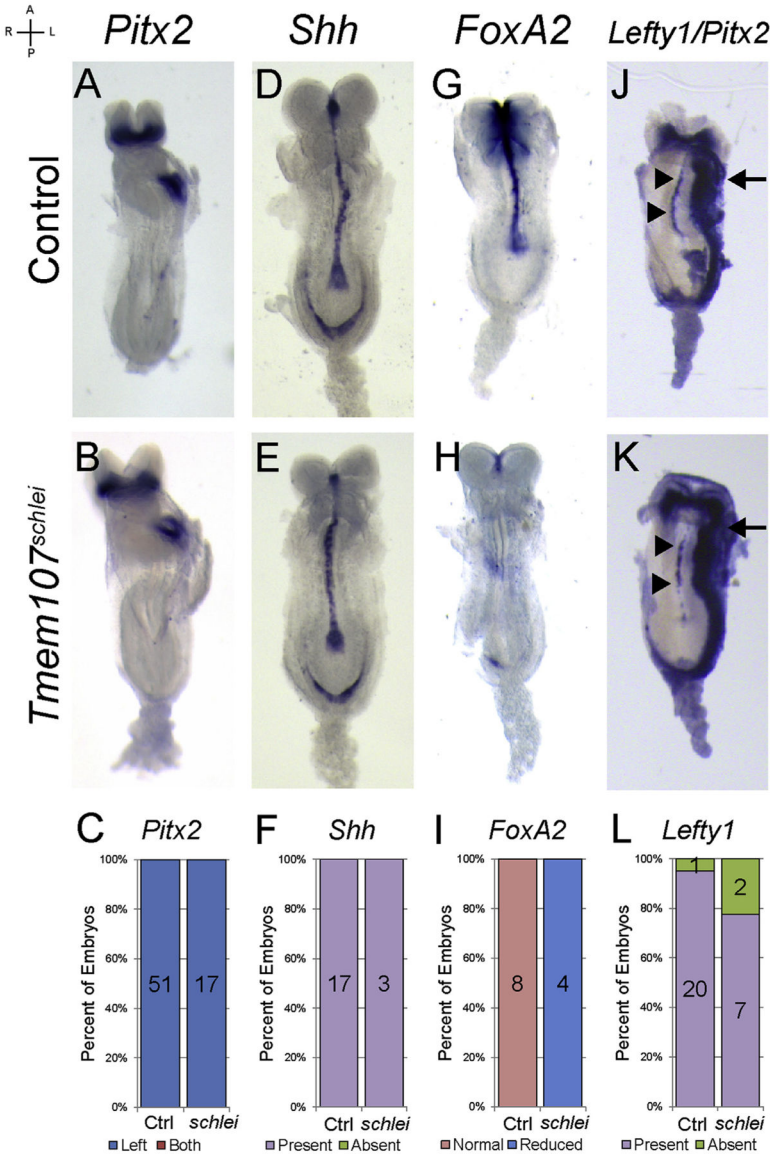

Fig. 6. *Tmem107*^{schlei} embryos maintain left-right asymmetry despite reduced SHH signaling in the midline.

(A, B) *in situ* hybridizations for *Pitx2* in control (A) and *Tmem107*^{schlei} (B) embryos show normal expression in the left LPM (D, E) *in situ* hybridization for *Shh* in control (D) and *Tmm107*^{schlei} (E) embryos, showing normal midline expression in both cases. (G, H) *FoxA2 in situ* hybridization is normal in controls (G) but is strongly reduced in the midlines of *Tmm107*^{schlei} (H) embryos. (J, K) Double *in situ* hybridization for *Lefty1* (midline, arrowheads) and *Pitx2* (LPM, arrows) revealed *Lefty1* expression in the midlines of *Tmem107*^{schlei} (K, arrowheads) embryos, albeit faint and/or patchy. (C, F, I, L) Graphs accompanying each probe represent the quantification of the embryos with a given expression pattern.

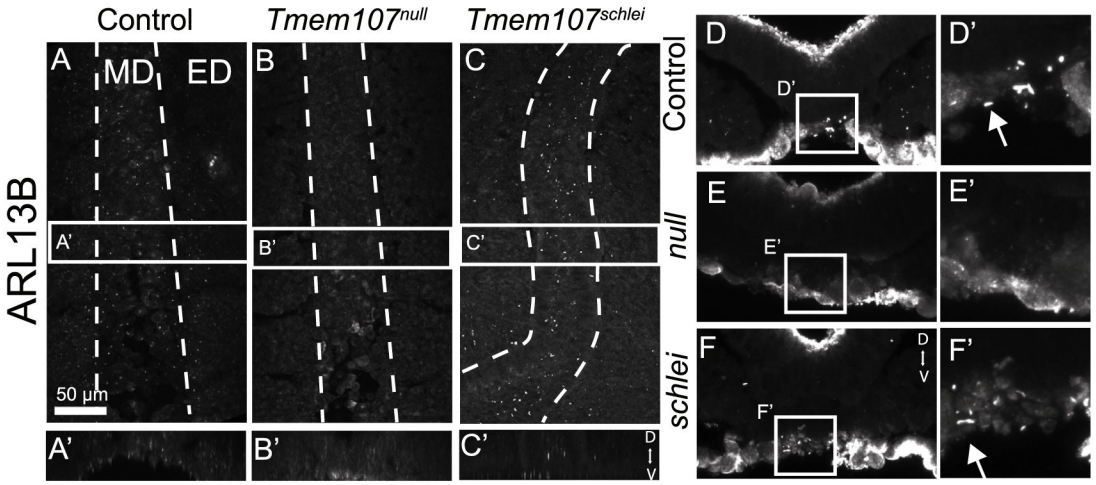

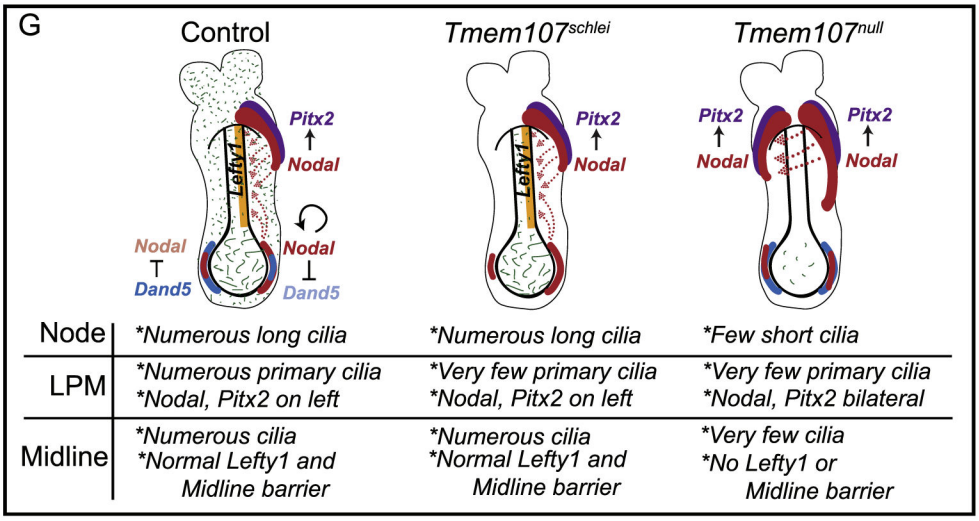

Fig. 7. Absence of cilia in the midline correlates with the laterality defects.

(A–C) Maximum intensity projected Z-stacks of confocal immunofluorescent images of E8.0 midlines using ARL13B as a cilia marker. Dashed lines outline the midline area. (A) Control embryos have numerous cilia in the midline (MD) and the surrounding endoderm (ED) (A′) Projected optical section of the boxed region in (A) shows widespread cilia.. (B) Only occasional cilia can be observed in the midlines of *Tmem107*^{null} embryos. (B′) Projected optical section of the boxed region in (B) shows few cilia. (C) A large population of ARL13 B positive cilia is consistently observed in the midline of *Tmem107*^{schlei} embryos. (C′) Projected optical section of the boxed region in (C) shows presence of cilia. (D–F) Confocal immunofluorescent images of sectioned E8.0 midlines, using ARL13B as a cilia marker. (D′-F′) Regions boxed in (D–F) focus on the prospective notochord that shows cilia in the control (D′, arrow) and *Tmem107*^{schlei} (F′, arrow), but not in *Tmem107*^{null} embryos (E′). Scale bar is 50 μm. (G) Summary diagram of key differences between the control and the two *Tmem107* mutants.

5.5.

Key resources table

Reagent or resource	Source	Identifier
Antibodies		
Rabbit polyclonal anti-PC2	Stefan Somlo (Cai et al., 1999)	
Rabbit polyclonal anti-ARL13B	Tamara Caspary (Caspary et al., 2007)	
Mouse monoclonal anti-ARL13B	UC Davis/NIH NeuroMab	ab136648
Chicken polyclonal anti-GFP Secondary antibodies: See Supplementary Methods Bacterial and Virus Strains	Abcam	ab13970
Biological Samples Mouse embryos	This paper, see Experimental Models	
Chemicals, Peptides, and Recombinant Proteins Critical Commercial Assays		
Deposited Data		
Experimental Models: Cell Lines		
Experimental Models: Organisms/Strains		
B6; 129S5(Cg)-Tmem107^{tm1Lex}/Mmucd	Lexicon (Tang et al., 2010)	MGI:5433209
Pkd2^{tm2Som} Genetic background: Involves: 129/Sv*129S2/ SvPas*C56BL/6*SJL	Stefan Somlo (Wu et al., 1998)	MGI:1860866
B6; C3Fe.B6-Tmem107^{schlei}	This study, (Christopher et al., 2012)	MGI:5433051
Dnah11^{tm11Bknr} Genetic Background: Involves 129S1/Sv*FVB/N*C56BL/6 Oligonucleotides See Supplementary Methods Recombinant DNA	Martina Brueckner (McGrath et al., 2003)	MGI:3623 683
In situ construct: Tmem107-pCRII- TOPO	This paper	
Full-length mouse *Tmem107* (NM_025838.2) Software and Algorithms		
Carl Zeiss AxioVision Product Suite	Zeiss	
Other		